

Enhanced cold mercury atom production with two-dimensional magneto-optical trap

Ye Zhang(张晔)1,2,3, Qi-Xin Liu(刘琪鑫)1,2,3, Jian-Fang Sun(孙剑芳)1,2,3, Zhen Xu(徐震)1,2,3,†, and Yu-Zhu Wang(王育竹)1,2,3

Citation: Chin. Phys. B, 2022, 31 (**7**): 073701. DOI: 10.1088/1674-1056/ac5397
Journal homepage: http://cpb.iphy.ac.cn; http://iopscience.iop.org/cpb

What follows is a list of articles you may be interested in

Optimization of a magneto-optic trap using nanofibers

Xin Wang(王鑫), Li-Jun Song(宋丽军), Chen-Xi Wang(王晨曦), Peng-Fei Zhang(张鹏飞), Gang Li(李刚), Tian-Cai Zhang(张天才)

Chin. Phys. B, 2019, 28 (**7**): 073701. DOI: 10.1088/1674-1056/28/7/073701

Loss of cold atoms due to collisions with residual gases in free flight and in a magneto-optical trap

Jing-feng Xiang(项静峰), He-nan Cheng(程鹤楠), Xiang-kai Peng(彭向凯), Xin-wen Wang(王新文), Wei Ren(任伟), Jing-wei Ji(吉经纬), Kang-kang Liu(刘亢亢), Jian-bo Zhao(赵剑波), Lin Li(李琳), Qiu-zhi Qu(屈求智), Tang Li(李唐), Bin Wang(汪斌), Mei-feng Ye(叶美凤), Xin Zhao(赵鑫), Yuan-yuan Yao(姚媛媛), De-Sheng Lü(吕德胜), Liang Liu(刘亮)

Chin. Phys. B, 2018, 27 (**7**): 073701. DOI: 10.1088/1674-1056/27/7/073701

Development of adjustable permanent magnet Zeeman slowers for optical lattice clocks

Xiao-Hang Zhang(张晓航), Xin-Ye Xu(徐信业)

Chin. Phys. B, 2017, 26 (**5**): 053701. DOI: 10.1088/1674-1056/26/5/053701

BaF radical: A promising candidate for laser cooling and magneto-optical trapping

Liang Xu(许亮), Bin Wei(魏斌), Yong Xia(夏勇), Lian-Zhong Deng(邓联忠), Jian-Ping Yin(印建平)

Chin. Phys. B, 2017, 26 (**3**): 033702. DOI: 10.1088/1674-1056/26/3/033702

Direct loading of atoms from a macroscopic quadrupole magnetic trap into a microchip trap

Jun Cheng(程俊), Jing-fang Zhang(张敬芳), Xin-ping Xu(许忻平), Hai-chao Zhang(张海潮), Yu-zhu Wang(王育竹)

Chin. Phys. B, 2017, 26 (**3**): 033701. DOI: 10.1088/1674-1056/26/3/033701

Enhanced cold mercury atom production with two-dimensional magneto-optical trap

Ye Zhang(张晔)[1,2,3], Qi-Xin Liu(刘琪鑫)[1,2,3], Jian-Fang Sun(孙剑芳)[1,2,3], Zhen Xu(徐震)[1,2,3,†], and Yu-Zhu Wang(王育竹)[1,2,3]

[1] *Shanghai Institute of Optics and Fine Mechanics, Chinese Academy of Sciences, Shanghai* 201800, *China*
[2] *Key Laboratory of Quantum Optics, Chinese Academy of Sciences, Shanghai* 201800, *China*
[3] *University of Chinese Academy of Sciences, Beijing* 100049, *China*

(Received 7 December 2021; revised manuscript received 22 January 2022; accepted manuscript online 10 February 2022)

A cold atom source is important for quantum metrology and precision measurement. To reduce the quantum projection noise limit in optical lattice clock, one can increase the number of cold atoms and reduce the dead time by enhancing the loading rate. In this work, we realize an enhanced cold mercury atom source based on a two-dimensional (2D) magneto-optical trap (MOT). The vacuum system is composed of two titanium chambers connected with a differential pumping tube. Two stable cooling laser systems are adopted for the 2D-MOT and the three-dimensional (3D)-MOT, respectively. Using an optimized 2D-MOT and push beam, about 1.3×10^6 atoms, which are almost an order of magnitude higher than using a pure 3D-MOT, are loaded into the 3D-MOT for ^{202}Hg atoms. This enhanced cold mercury atom source is helpful in increasing the frequency stability of a neutral mercury lattice clock.

Keywords: magneto-optical trap, atomic beam, neutral mercury atom, laser cooling and trapping

PACS: 37.10.De, 37.10.Gh, 06.30.Ft **DOI:** 10.1088/1674-1056/ac5397

1. Introduction

With the development of laser cooling and trapping techniques, cold atoms are now widely used in quantum simulation, quantum computation, and precision measurement. One of the important applications is cold atoms-based frequency standards, including microwave clocks and optical clocks. To improve the performance of an atomic clock, it is necessary to reduce the dead time by increasing the loading rate of cold atom in the 3D-MOT. On the other hand, it is important to maintain a relatively long lifetime of cold atoms in optical lattice, which requires an ultra-high vacuum in the science chamber. There are two widely used pre-loading schemes to increase the loading rate of a 3D-MOT. One is the Zeeman slower, which is adopted in many cold atom setups, especially in those atoms with low saturated vapor pressure at room temperature, such as the strontium and the ytterbium atoms. The other is the 2D-MOT, which generates low velocity atomic flux by laser cooling from a vapor cell or by laser collimation from a thermal beam. It has the advantages of compactness, versatility, good collimation, and isotope selection. It avoids long decelerating tube, large Zeeman coil, residual thermal atomic beam, and mechanical shutter, so it is popularly used in the research of cold atom physics. Several different configurations[1–4] have been demonstrated, and these have been used in atomic fountain,[5] atom interferometry,[6] and quantum gases[7] for alkali atoms[8–11] and alkali-earth-like atoms.[12] Recently, it has also been demonstrated that atomic flux can be enhanced by multi-frequency or sideband frequency 2D-MOT.[13,14]

Nevertheless, each kind of element has its specific merit and difficulty as well for laser cooling. Even though the 2D-MOT configuration has been widely used in alkali atoms and alkali-earth-like atoms, the application in mercury (Hg) atoms is still difficult. Firstly, the vapor pressure of Hg atoms at room temperature is much higher than that of other metal atoms. It is necessary to use a two-chamber system to achieve a high vacuum in the science chamber. Secondly, the natural line-width of cooling transition for mercury atoms is $\Gamma = 1.27$ MHz, which is narrower than those for alkali-metal atoms (Rb/Cs/K/Li, about 6 MHz) and alkali-earth-like atoms (Sr/Yb about 30 MHz), and the capture velocity range of the 3D-MOT is smaller. Finally, compared with others, the cooling transition at 253.7 nm is in the deep ultra-violet (DUV) region. Although it can be obtained through frequency quadrupling from a high power infrared laser,[15–19] maintaining a high power and continuous output is still difficult.

Although there are many technical challenges, mercury is still selected as a candidate of optical frequency standard, and it is recommended as one of the secondary representations of second by BIPM[20] due to its low sensitivity to black-body radiation. It has been laser-cooled and loaded into a magic wavelength optical lattice, and its absolute frequency has been determined by primary fountain clock and also by Sr/Yb optical lattice clock.[21–23] It is attractive for its higher sensitivity to test the variation of fine-structure constant.[24] At present, the stability is limited mainly by its long cycle time, which

†Corresponding author. E-mail: xuzhen@mail.siom.ac.cn
© 2022 Chinese Physical Society and IOP Publishing Ltd

makes it particularly important to achieve a faster production of cold mercury atoms.

In this work, we report an experiment on enhancing the production of cold mercury atom source for neutral mercury lattice clock, which effectively improves the loading rate of mercury cold atoms with optimized 2D-MOT and push beam. A smart light path arrangement is used to solve the problem of insufficient DUV light. Two stable cooling laser systems are used for 2D-MOT and 3D-MOT, respectively. One for 2D-MOT is frequency stabilized at atomic spectrum of 253.7 nm, and the other for 3D-MOT is locked on the former by optical frequency locked loop. After optimizing the detuning and the power of 2D-MOT beam and push beam, about 1.3×10^6 mercury atoms are loaded into the 3D-MOT for ^{202}Hg, corresponding to a loading rate of 1.0×10^6 atoms/s. Using the 2D-MOT and the push beam, the loading rate is enhanced by a factor of 8.4 higher than using the pure 3D-MOT. This cold mercury atom source will be used in mercury lattice clock, which can effectively shorten the cycle time in a clock operation.

2. Experimental setup

The vacuum system is mainly composed of an Hg-source chamber, a 2D-MOT chamber and a science chamber. The 2D-MOT and the science chambers are made of nonmagnetic titanium alloy to avoid unpredictable magnetic field. The homemade Hg-source is cooled to -41 °C to keep a relatively low vapor pressure. More details are described in our previous work.[25] In order to maintain a relatively high vacuum in the 2D MOT chamber, an ion pump with a pumping speed of 3 L/s is placed at the end of the mercury source chamber, and finally a vacuum of 2×10^{-8} Torr (1 Torr = 1.33322×10^2 Pa) is achieved in the 2D-MOT chamber.

The 2D-MOT chamber has four UV fused silica (UVFS) windows each with a clear aperture of 20 mm in diameter as shown in Fig. 1. A pair of elongated coils are mounted on the 2D-MOT chamber, and produce a 2D quadruple magnetic field for the 2D-MOT. The magnetic field gradient is about 25 Gs/cm (1 Gs = 10^{-4} T). Two windows in the x direction are used for push beam.

The science chamber and the 2D-MOT chamber which have a distance of 11 cm in between are connected by a differential pumping tube. The differential pumping tube is 30-mm long, which includes a 12-mm-long tube with 1.5-mm inner diameter and a conical nozzle. The conical nozzle is gold plated to reduce the vapor pressure of mercury atoms in the science chamber based on the adsorption of gold to mercury. The science chamber is connected to an ion pump with a pumping speed of 40 L/s, and finally has a vacuum of 2×10^{-10} Torr. A pair of anti-Helmholtz coils are mounted on the science chamber to produce the magnetic field for 3D-MOT, and the gradient is about 15 Gs/cm in the center. Three pairs of rectangular coils are used to compensate for the geomagnetic field to lower than 10 mG.

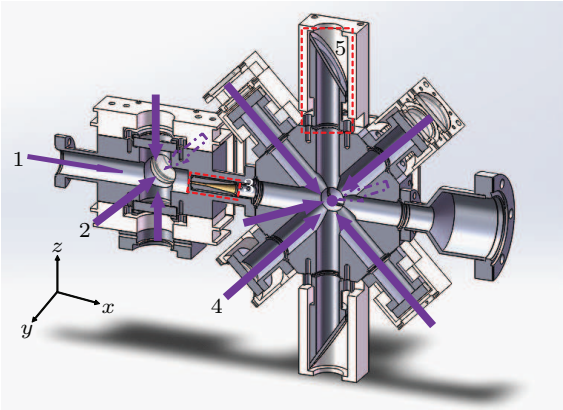


Fig. 1. Apparatus of 2D-MOT and 3D-MOT. 1: push beam; 2: 2D-MOT beam (single folded path); 3: differential pumping tube; 4: 3D-MOT beams; 5: Brewster windows.

To ensure the laser power at 253.7 nm and to conveniently tune the frequency of the two cooling lasers, we use two homemade deep ultraviolet (DUV) lasers at 253.7 nm as the cooling laser for 2D-MOT and 3D-MOT, respectively.[26] In order to maintain a long-term operation, we operate the DUV laser for 3D-MOT at relatively low power of 80 mW, even though each of these two lasers can generate output power more than 100 mW. A 50-μm pin-hole is used to reshape the DUV beam. Then the light is split into three beams, each with a radius of 4 mm and maximum power of 14 mW. Each beam is reflected after a quarter wave plate to form a standard six-beam configuration for a 3D-MOT. Compared with our earlier work with folded single-beam 3D-MOT,[27] this configuration can improve the intensity balance between the counter-propagating cooling beams.

The DUV laser for the 2D-MOT is operated at 40 mW. After the spatial filter with a pin-hole and beam shaping with cylindrical lenses, the cooling beam has a size of about 10 mm×8 mm. In order to maximize the intensity of the cooling laser for the 2D-MOT, a single beam-folded configuration is adopted, and a maximum intensity of $5I_{\rm SAT}$ is reached, where $I_{\rm SAT}$ is 10.2 mW/cm^2. The rest of the DUV light is used for the frequency modulation saturated absorption spectroscopy (SAS) locking and push beam as shown in Fig. 2. In this configuration, the independent operation for the detuning of cooling laser and push beam can be achieved by adjusting the frequencies of these three AOMs. After locking the frequency of the 2D-MOT cooling laser on SAS, the frequency of 3D-MOT cooling laser is adjusted by an optical frequency locking loop (OFLL)[28] between the two fundamental seed lasers. The atom number in 3D-MOT is counted by fluorescence image on an electron multiplying CCD (EMCCD, Andor, iXon3 885). Four galvanometers are used to switch the push beam, the cooling beams for 2D-MOT and 3D-MOT for time sequence as shown in Fig. 2.

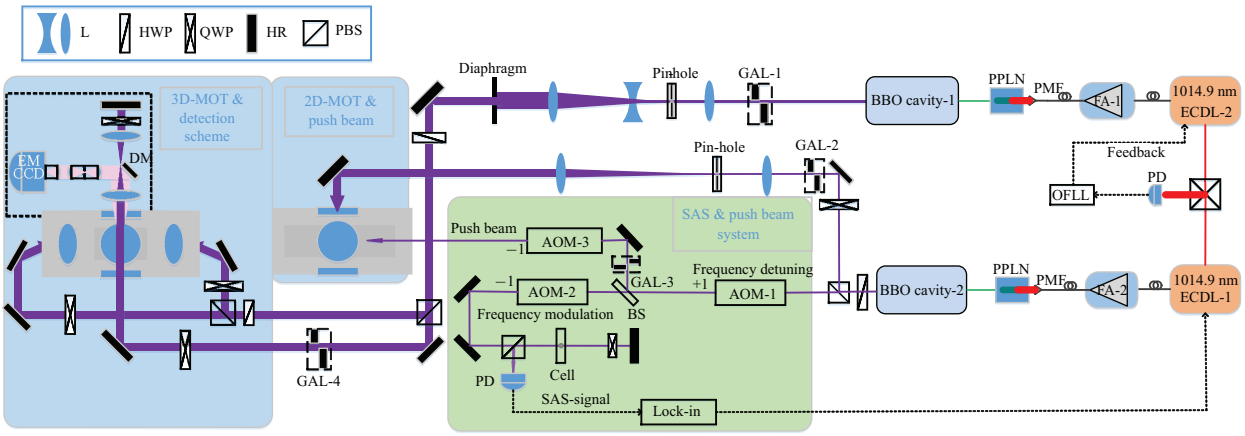


Fig. 2. Schematic diagram of cold mercury atom laser system. ECDL: external cavity diode laser; AOM: acousto-optical modulator; BS: beam splitter; HR: high reflection mirror; FA: fiber laser amplifier; PMF: polarization-maintained fiber; HWP: half wave plate; QWP: quarter wave plate; PD: photodiode; PBS: polarizing beam splitter; DB: dichroic beam splitter; PZT: piezo transducer; GAL: galvanometer; L: lens; DM: "D" shaped mirror; EMCCD: electron multiplying charge couple device.

3. Enhanced production of cold mercury atom

The atom number N in a 3D-MOT can be calculated from the following rate equation:[29]

$$\frac{\mathrm{d}N}{\mathrm{d}t} = R - \gamma N, \tag{1}$$

where R is the loading rate and $\gamma$is the loss rate of the 3D-MOT. The loading rate is normally influenced by the capture range of the 3D-MOT and the flux of the atom source. In this configuration, the atom source is determined by the performance of the 2D-MOT. The saturated atom number reaches $N_0 = R/\gamma$. If $N = 0$ at $t = 0$, the atom number at time t is

$$N(t) = N_0\left(1 - \mathrm{e}^{-\gamma t}\right). \tag{2}$$

With the above setup, we capture the cold atoms in the science chamber, and the enhancement effect is observed with the help of the 2D-MOT and the push beam. For the 3D-MOT, each cooling laser beam has an intensity of $2.8I_{\mathrm{SAT}}$, the detuning is optimized to be -8Γ, and the magnetic gradient is optimized to be 15 Gs/cm. With these parameters, we use the loading rate and the saturated atom number to optimize the 2D-MOT performance. To detect the atom number by the fluorescence detection, the detuning of detection laser is tuned to -2Γ, and a 6-ms pulse of detection light is incident into the cold atoms in the x–z plane after having switched off the cooling laser in the y direction.

The capture velocity for laser cooling can be described as[30]

$$v_{\mathrm{c}} = \sqrt{\frac{\hbar k\Gamma}{2m}}r_{\mathrm{c}}, \tag{3}$$

where $\hbar$ is the Planck constant, k is the wave vector, m is the mass of a ^{202}Hg atom, and r_{c} is the radius of the cooling beam. According to the parameters used in the experiment, the capture velocity is 5 m/s. Since the most probable velocity of mercury atoms is 157 m/s at room temperature, and the atoms in a mercury vapor obey the Maxwell–Boltzmann velocity distribution, very few atoms are in the velocity range of 0 m/s–5 m/s. Therefore, the loading rate of the 3D-MOT is much lower than that without the help of atomic flux from the 2D-MOT.

Figure 3 shows a typical loading process of cold mercury atom in the 3D-MOT. The loading rate and saturated atom number in the 3D-MOT effectively increase with the help of the 2D-MOT beam and the push beam as shown in Table 1. The loading rate of the 3D-MOT increases by a factor of 3.1 with using the 2D-MOT beam, and by a factor of 8.4 with using both the 2D-MOT beam and the push beam. The optimized loading rate is 1.0×10^6 atoms/s, and the saturated atom number is 1.3×10^6.

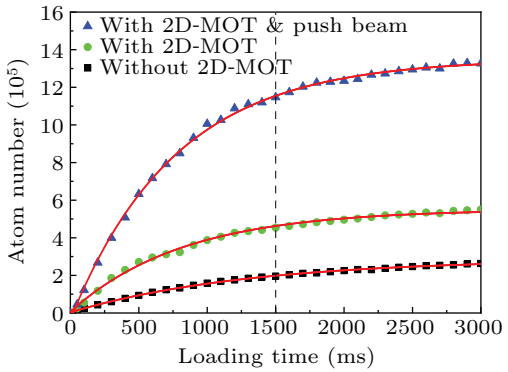


Fig. 3. 3D-MOT loading curves with using both of and neither of 2D-MOT and push-beam.

Table 1. Atom number, loading rate and loss rate in the 3D-MOT.

	Atom number at 3 s	Loading rate (atoms/s)	Loss rate (/s)
3D-MOT only	2.4×10^5	1.2×10^5	0.75
With 2D-MOT	5.2×10^5	3.7×10^5	1.00
With 2D-MOT + push beam	1.3×10^6	1.0×10^6	1.35

The effective enhancement of the loading rate depends on the optimization of the parameters of the 2D-MOT. Several key factors affect the loading process in the 3D-MOT, such as the intensity and the detuning of the 2D-MOT beam. Because of the limited cooling laser power and optical windows, the size of the 2D-MOT beam is 10 mm×8 mm and the laser intensity is $5I_{\rm SAT}$. The magnetic field gradient is 25 Gs/cm so as to maximize the capture velocity. The 2D-MOT captures and collimates the mercury atoms to form an intense atom flux with low transversal velocity. The detuning of the 2D-MOT beam is optimized to enhance the loading rate of 3D-MOT, which is influenced by the capture rate and the transverse temperature of 2D-MOT. For a bigger detuning, normally it has a larger capture range for 2D-MOT under a certain magnetic field gradient. And the Doppler cooling theory indicates that[31] for a smaller detuning it has a smaller transverse temperature, *i.e.* a smaller transverse velocity. Therefore, more atoms in the 2D-MOT can pass through the differential pumping tube. As shown in Fig. 4, the optimized detuning of the 2D-MOT beam is determined to be -4Γ. Considering the capture range of the 3D-MOT, the total atomic flux is estimated at 4×10^7 atoms/s.

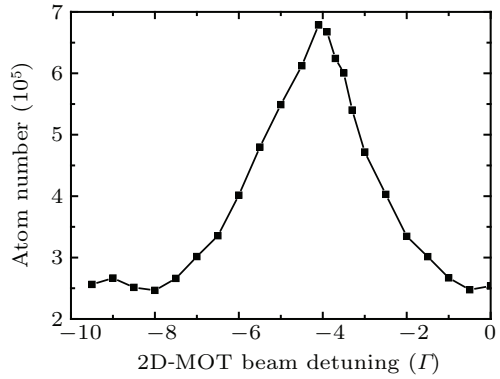


Fig. 4. Characterization of atom number *versus* 2D-MOT beam detuning, with loading time being 1.5 s.

Although the loading rate of the 3D-MOT improves with using the 2D-MOT setup, it can be further enhanced with using the push beam. The diameter of push beam is about 1.5 mm, which is close to the size of differential pumping tube. The scattering force of the push beam drives some atoms to change their longitudinal velocities and then they can fly into the 3D-MOT area. Since the scattering force of the push beam on the atoms is regarded as being in the longitudinal direction of the 2D-MOT, we take the motion of atom as one-dimensional motion in simulation. According to the theory of laser cooling, the scattering force[32] is

$$F_{\rm sc} = \frac{\hbar k\Gamma}{2}\frac{s}{1+s+4(\Delta/\Gamma)^2}, \tag{4}$$

where $s = I/I_{\rm SAT}$, I is the laser intensity, $\Delta = \delta - k\cdot v_z$, δ is the laser detuning, v_z is the velocity of mercury atom in the z direction. The scattering force is determined by the laser detuning, laser power and the velocity of atom. To analyze how it works on the atom, we trace the atoms with different initial longitudinal velocities as shown in Fig. 5, and we find that some atoms with negative velocities can be driven into the atoms with positive velocities. If the final velocity is larger than the capture velocity of the 3D-MOT, the atoms cannot be loaded into the 3D-MOT. And if the initial velocity is too large, the atoms will run out of the region of the 2D-MOT backward, and then the atoms cannot go through the differential pumping tube. So some atoms within special velocity region can be pushed into the 3D-MOT, and the loading rate is enhanced.

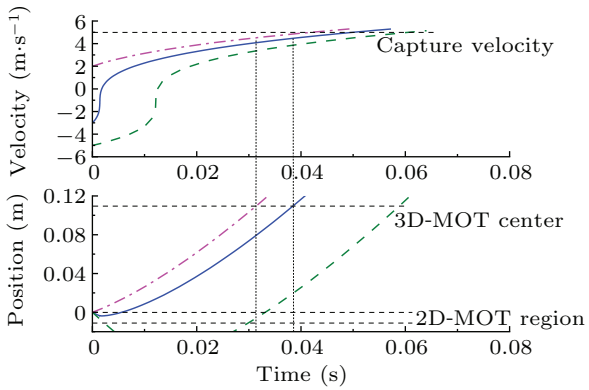


Fig. 5. Simulations of the velocity and the position of atoms at different initial velocities when detuning is 3.5Γ and intensity is $2I_{\rm SAT}$.

Apparently, the detuning of push beam plays an important role in determining which atoms can be pushed into the 3D-MOT. We trace an atom with an initial velocity of 3 m/s varying with different detunings, and the results are shown in Fig. 6(a). If the detuning is too small, even more atoms will be pushed into the region of positive velocity, *i.e.* original atoms with negative velocity turn into the atoms with positive velocity, but the final velocity will exceed the capture velocity of 3D-MOT. If the detuning is too large, the final velocity will be too small, or kept on the negative velocity side, *i.e.*, these atoms cannot enter into the 3D-MOT region. Considering these effect, an appropriate detuning can maximize the loading rate of the 3D-MOT. Because the natural line-width of mercury atom is rather smaller than that of alkali atom, the capture velocity is relatively small, and therefore the range of the optimized detuning is a little bit narrow.

Another key effect is caused by the laser intensity as shown in Fig. 6(b). When the laser power is too weak, the atoms will run out of the 2D-MOT region before its velocity turns positive, so the atoms cannot enter into the science chamber. As the laser power increases, the atoms can be turned into the atoms with a positive velocity in the 2D-MOT region, and finally captured by the 3D-MOT. But the scattering force will be saturated according to formula (4), and the final velocity will be out of the capture velocity of the 3D-MOT. Therefore, when the laser power increases, not only more atoms will turn over to the 3D-MOT, but also they have greater possibility to be pushed out of the capture velocity.

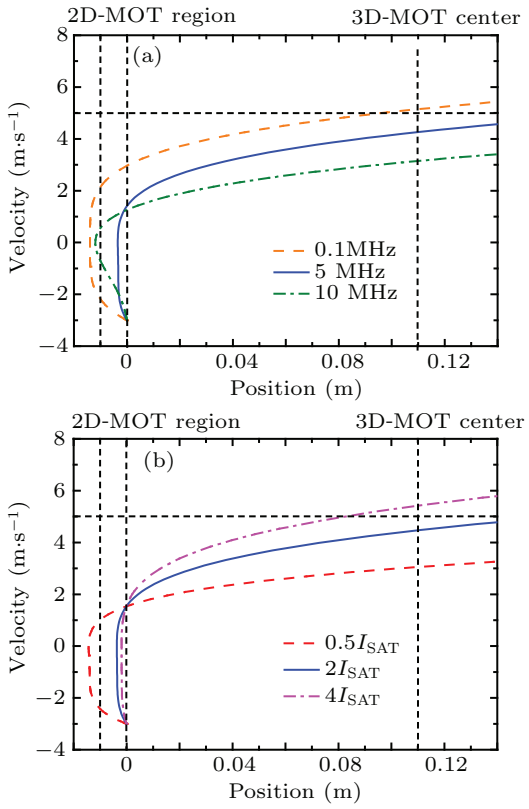


Fig. 6. Simulations of movement of atoms at (a) $s = 1.7I_{SAT}$ and (b) $\delta = 4.5$ MHz.

To optimize the push beam, we measure the cold atom number and the results are shown in Fig. 7. The optimized power is about 0.35 mW, which corresponds to $1.7I_{SAT}$. The atom number increases linearly with the laser power of the push beam increasing. But with the laser power being above the optimized power, the atom number is not obviously enhanced. And the optimized detuning of push beam is -3.5Γ. The atom number decreases on both sides of the optimized detuning.

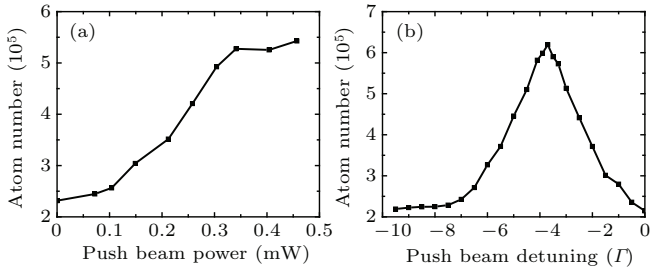


Fig. 7. Characterization of 2D-MOT depending on (a) push beam power and (b) push beam detuning.

The experimental results in Table 1 show that the loss rate increases as the loading rate increasing. The loss is normally caused by the collisions of background gases, the atom beam, the scattering light, and the push beam. Owing to the low atom number, *i.e.* low density of atoms in the 3D MOT, the collision between cold atoms is negligible. The collision between the cold atoms and the background gases is the main reason for the loss in 3D-MOT. As shown in Table 1, the loss from background gases is determined to be 0.75/s. With the 2D-MOT beam, the loss rate is about 1.0 s^{-1}, and the increased loss probably comes from the collimated atomic beam. Because the atomic beam is collimated and roughly aims at the center of the 3D-MOT region, the collision happens frequently between the high velocity mercury atoms from the atomic beam and the cold atoms in the 3D-MOT. With using the 2D-MOT and the push beam, the additional loss is from the push beam, because its frequency is not far from the transition frequency of cold atoms.

As discussed above, although the loading rate is increased by a factor of 8.4 with using the 2D-MOT and the push beam, the loss rate is also enlarged 1.8 times, which is attributed mainly to the interactions between the collimated atomic beam and the push beam on the cold atom in the 3D-MOT. This kind of loss can be removed by displacing the 3D-MOT away from the intense atomic beam and the push beam, which has already been used in some experiments,[7] so that the saturated atom number can be further increased. Unfortunately, we cannot use this method in our experiment, because it requires a larger capture area, *i.e.* a larger cooling beam. Nevertheless, the enhanced loading rate shortens the loading time to 100 ms for the preparation of 10^5 cold atoms, which is valuable to a neutral mercury lattice clock in the future.

4. Conclusions

In this paper, we build a setup to produce cold mercury atoms, in which the configuration of the 2D-MOT plus the push beam is adopted. The collimated atomic flux from the 2D-MOT can effectively enhance the loading rate, and it can prevent too much atoms out of the higher mercury vapor chamber from directly entering into the science chamber. So it improves the vacuum. With this setup, the loading rate of ^{202}Hg atoms is increased by a factor of 8.4, and about 1.3×10^6 mercury atoms are loaded into the 3D-MOT. The enhancement of the loading rate can effectively shorten the loading time, which is beneficial to reducing the dead time of optical clock. It is important to reduce the quantum projection noise limit. We can make some modifications to improve the performance of the 2D-MOT in the future, such as extending the cooling length of the 2D-MOT with an upgraded DUV laser. This device will be applied to our neutral mercury optical lattice clock, which will play an important role in improving the stability of the clock.

References

[1] Lu Z T, Corwin K L, Renn M J, Anderson M H, Cornell E A and Wieman C E 1996 *Phys. Rev. Lett.* **77** 3331
[2] Schoser J, Bat A, R L, Schweikhard V and Pfau T 2002 *Phys. Rev. A* **66** 023410
[3] Dieckmann K, Spreeuw R, M Weidemüller and Walraven J 1998 *Phys. Rev. A* **58** 3891
[4] Catani J, Maioli P, Sarlo L D, Minardi F and Inguscio M 2006 *Phys. Rev. A* **73** 033415
[5] Wu C J, Jun R, Jiang C, Hui Z and Zhang S G 2013 *Acta Phys. Sin.* **62** 063201 (in Chinese)

[6] Muller T, Wendrich T, Gilowski M, Jentsch C, Rasel E M and Ertmer W 2007 *Phys. Rev. A* **76** 063611

[7] Dorscher S, Thobe A, Hundt B, Kochanke A, Targat, Windpassinger, Becker C and Sengstock K 2013 *Rev. Sci. Instrum.* **84** 043109

[8] Chen Y D, Li W X, Chou M E, Kuo C H and Tung S 2021 *Phys. Rev. A* **103** 023102

[9] Chaudhuri S, Roy S and Unnikrishnan C S 2006 *Phys. Rev. A* **74** 023406

[10] Tiecke T G, Gensemer S D, Ludewig A and Walraven JTM 2009 *Phys. Rev. A* **80** 013409

[11] Shanchao Z, Chen J F, Liu C, Zhou S Y, Loy M M T, Wong G K L and Du S W 2012 *Rev. Sci. Instrum.* **83** 073102

[12] Nosske I, Couturier L, Hu F, Tan C and Weidemüller M 2017 *Phys. Rev. A* **96** 039901

[13] Li K, Zhang D, Gao T, Peng S G and Jiang K 2015 *Phys. Rev. A* **92** 013419

[14] Barbiero M, Tarallo M G, Calonico D, Levi F and Ferrari G 2019 *Phys. Rev. Appl.* **13** 014013

[15] Scheid M, Markert F, Walz J, Wang J Y, Kirchner M and Hansch T W 2007 *Opt. Lett.* **32** 955

[16] Paul J, Kaneda Y, Wang T L, Lytle C and Jones R J 2011 *Opt. Lett.* **36** 61

[17] Hachisu H, Miyagishi K, Porsev S G, Derevianko A, Ovsiannikov V D, Pal'Chikov V G, Takamoto M and Katori H 2008 *Phys. Rev. Lett.* **100** 053001

[18] Steinborn R, Koglbauer A, Bachor P, Diehl T and Kolbe D 2013 *Opt. Express* **21** 022693

[19] Hu J M, Zhang L, Liu H, Liu K, Xu Z and Feng Y 2013 *Opt. Express* **21** 030958

[20] https://www.bipm.org/en/publications/mises-en-pratique/standard-frequencies-second

[21] Yamanaka K, Ohmae N, Ushijima I, Takamoto M and Katori H 2015 *Phys. Rev. Lett.* **114** 230801

[22] Noriaki O, Filippo B, Nils N and Hidetoshi K 2020 *Opt. Express* **28** 015112

[23] Tyumenev R, Favier M, Bilicki S, Bookjans E, Targat R L, Lodewyck J, Nicolodi D, Coq Y L, Abgrall M and Guéna J 2016 *New J. Phys.* **18** 113002

[24] Porsev S G and Derevianko A 2006 *Phys. Rev. A* **74** 020502

[25] Liu H L, Yin S Q, Liu K K, Qian J, Xu Z, Hong T and Wang Y Z 2013 *Chin. Phys. B* **22** 043701

[26] Zhang Y, Liu Q, Fu X H, Sun J F, Xu Z and Wang Y Z 2021 *Opt. Laser Technol* **139** 106956

[27] Liu K K, Zhao R C, Gou W, Fu X H, Liu H L, Yin S Q, Sun J F, Xu Z and Wang Y Z 2016 *Chin. Phys. Lett.* **33** 070602

[28] Lipka M, Parniak M and Wasilewski W 2017 *Appl. Phys. B* **123** 238

[29] Gibble K E, Kasapi S and Chu S 1992 *Opt. Lett.* **17** 526

[30] Steane A M, Chowdhury M and Foot C J 1992 *J. Opt. Soc. Am. B* **9** 2142

[31] McFerran J J, Yi L, Mejri S and Bize S 2010 *Opt. Lett.* **35** 003078

[32] Metcalf H J and Straten P V D 1999 *Laser Cooling and Trapping* (New York: Springer) p. 88